

The geometric effects of ${}^{\vee}\text{Fe}^{2+}$ for ${}^{\vee}\text{Mg}$ substitution on the crystal structures of the grandidierite-omineite series

TASHIA J. DZIKOWSKI,¹ LEE A. GROAT,^{1,*} AND EDWARD S. GREW²

¹Department of Earth and Ocean Sciences, University of British Columbia, 6339 Stores Road, Vancouver, British Columbia V6T 1Z4, Canada

²Department of Geological Sciences, University of Maine, 5790 Bryand Research Center, Orono, Maine 04469-5790, U.S.A.

ABSTRACT

The electron microprobe compositions and crystal structure of seven members of the grandidierite-omineite ($\text{MgAl}_3\text{BSiO}_9\text{-Fe}^{2+}\text{Al}_3\text{BSiO}_9$) series with $X = (\text{Fe}^{2+} + \text{Mn} + \text{Zn})/(\text{Fe}^{2+} + \text{Mn} + \text{Zn} + \text{Mg})$ ranging from 0.00 to 0.52 were studied to determine the geometric effects of Fe substitution for Mg on the crystal structures. Calculating Fe^{3+} from the electron microprobe analyses gave 0.04–0.06 Fe^{3+} apfu, but such small amounts at the Al sites could not be detected in the refinements. Regression equations derived from single-crystal X-ray diffraction data show that b increases by 0.18 Å from $X = 0$ –1. The crystal structure refinements show that the most significant changes involve the $(\text{Mg,Fe}^{2+})\text{O}_5$ polyhedron, which increases in volume by 0.36 \AA^3 (5.0%), largely as a result of expansion of the MgFe-O5 , -O2, and -O6 ($\times 2$) bond distances, which increase by 0.09 (4.4%), 0.06, and 0.04 Å, respectively. Other significant changes include increasing O1-MgFe-O2 (3.44°) and -Al3-O5a angles (1.9°) and a decreasing O6-MgFe-O6b (-2.20°) angle. Significant increases are also seen in the lengths of the O1-O2 (0.13 Å) and O6-O5a ($\times 2$) (0.09 Å) edges. The SiO_4 tetrahedra appear to respond to changes in the surrounding polyhedra by changing O-Si-O angles such that the tetrahedral angle variance and mean tetrahedral quadratic elongation increase with X . The BO_3 triangles appear to behave as relatively invariant units in the crystal structure.

Regression equations obtained from the MgFe-O bond distances were used to determine a radius for ${}^{\vee}\text{Fe}^{2+}$ of 0.70 Å. Although our samples show little Mn, the presence of Mn^{2+} at the MgFe site would be expected to cause more distortion than an equivalent amount of Fe^{2+} . Substitution of Zn likely would have little effect. The presence of Cr^{3+} at any of the Al sites would be expected to increase the size of the coordination sphere, but the substitution of P^{5+} for Si at the Si sites would most likely decrease the Si-O bond distances.

Keywords: Grandidierite, omineite, crystal structure, substitution, borosilicates

INTRODUCTION

Grandidierite, $(\text{Mg,Fe}^{2+})\text{Al}_3\text{BSiO}_9$, (Lacroix 1902; McKie 1965; Stephenson and Moore 1968) and its Fe^{2+} -dominant analog omineite, $(\text{Fe}^{2+},\text{Mg})\text{Al}_3\text{BSiO}_9$ (Hiroi et al. 2002), form a continuous series in which Fe^{2+} substitutes for Mg exclusively at a single fivefold-coordinated site. This relatively simple solid-solution series offers an unusual opportunity to study the changes in bond lengths and angles in a structure in which $\text{Fe}^{2+} = \text{Mg}$ substitution is restricted to a single site and other compositional variations are much subordinate. Few other minerals (e.g., farringtonite, graftonite, joaquinite, vesuvianite, werdingite, yoderite) are known to contain ${}^{\vee}\text{Mg}$ or ${}^{\vee}\text{Fe}^{2+}$, but in some of these what substitution has been found is complicated by the presence of other constituents. We undertook this study to characterize the geometric effects of ${}^{\vee}\text{Fe}^{2+}$ for ${}^{\vee}\text{Mg}$ substitution on the crystal structure of the grandidierite-omineite series, and to investigate the reasons for the apparent rarity of ${}^{\vee}\text{Mg}$ and ${}^{\vee}\text{Fe}^{2+}$ in minerals.

BACKGROUND

Grandidierite and omineite are relatively high-temperature, low-pressure minerals (mostly 500–800 °C, 0.3–7 kbar). These

P - T estimates are consistent with preliminary experimental data on the stability range for end-member grandidierite: Werding and Schreyer (1996) reported that its upper pressure stability limit is roughly coincident with that of sillimanite under nearly anhydrous conditions, but that this limit is shifted to lower pressures under excess- H_2O conditions. Grandidierite is found in granulite-facies pegmatites, migmatites, and regionally and contact metamorphosed pelitic and calcareous rocks at approximately 40 localities worldwide (e.g., Grew 1996; Grew et al. 1998a). The type locality for omineite is a porphyritic granite in Japan, but compositions with $\text{Fe}^{2+} \geq \text{Mg}$ have also been reported from a pegmatite at Almgjotheii, Norway [$X = \text{Fe}/(\text{Fe} + \text{Mg}) = 0.50$ –0.81, Huijsmans et al. 1982; Grew et al. 1998a], hornfels at Morton Pass, Wyoming ($X = 0.58$, Grant and Frost 1990) and at Bellerberg, Eifel, Germany ($X \approx 0.5$, Blass and Graf 1994), and in a regional aureole at Mt. Stafford, Australia ($X = 0.50$ –0.55, calculated from Greenfield et al. 1998).

Grandidierite and omineite belong to the family of B-Al-Si phases that includes boralsilite, synthetic $\text{Al}_8[(\text{Al,B})_{12}\text{B}_4]\text{O}_{33}$, and werdingite, all of which have structures based on chains of edge-sharing Al octahedra parallel to a lattice translation of ca. 5.6 Å (c in grandidierite and omineite). According to Peacor et al. (1999), the phases in this family differ from one another in

* E-mail: lgroat@eos.ubc.ca

the nature of the polyhedral units that cross-link the chains of AlO_6 octahedra. Fivefold-coordinated polyhedra are a common building block in the cross-linking units. In grandidierite and ominelite, the cross-linking units are $(\text{Mg},\text{Fe}^{2+})\text{O}_5$ and AlO_5 polyhedra, SiO_4 tetrahedra, and BO_3 triangles (Figs. 1 and 2). The $(\text{Mg},\text{Fe}^{2+})\text{O}_5$ polyhedron is a distorted trigonal bipyramid about the MgFe site, in which the long axis, which is defined by M (= MgFe)-O2 and M-O5 bonds about 180° apart, is approximately parallel to **b**. The other polyhedron of the dimer is an approximately parallel trigonal bipyramid about the Al3 site.

The $(\text{Mg},\text{Fe}^{2+})\text{O}_5$ and Al_3O_5 polyhedra and AlO_6 octahedra all have some edges that are shared. Each $(\text{Mg},\text{Fe}^{2+})\text{O}_5$ polyhedron shares two O2-O6 edges with two different Al_1O_6 octahedra and one O1-O5 edge with an Al_3O_5 polyhedron. Al_1O_6 octahedra share two O2-O3 edges with two adjacent Al_1O_6 octahedra and two O2-O6 edges with $(\text{Mg},\text{Fe}^{2+})\text{O}_5$ polyhedra. Every Al_2O_6 octahedron shares two O4-O5 edges with other Al_2O_6 octahedra and two O5-O7 edges with Al_3O_5 polyhedra. Finally, all Al_3O_5 polyhedra share one O1-O5 edge with an $(\text{Mg},\text{Fe}^{2+})\text{O}_5$ polyhedron and two O5-O7 edges with Al_2O_6 octahedra. It is interesting to note that in this case all of the shared edges meet at the same O5 atom at one end of the trigonal bipyramid.

Olesch and Seifert (1976) were the first to study the effects of increasing X on the crystallographic properties of grandidierite, including both synthetic and natural samples. They reported that b shows a strong positive correlation with X , whereas a and c remain essentially constant; therefore the expansion of the unit cell is anisotropic, and leads to increasing distortion of the $(\text{Mg},\text{Fe}^{2+})\text{O}_5$ polyhedron. Seifert and Olesch (1977) studied the ${}^{57}\text{Fe}$ Mössbauer spectrum of grandidierite and reported that the degree of distortion of the coordination polyhedron around the MgFe site can also be inferred from the hyperfine parameters. Farges (2001) collected Fe- K edge XAFS spectra from eight grandidierite samples from Madagascar and Zimbabwe. The pre-edge spectra were consistent with dominantly five-coordinated Fe^{2+} . Analysis of the XANES and EXAFS spectra confirmed that Fe^{2+}

substitutes for Mg in grandidierite with a slight expansion ($\sim 2\%$) of the local structure around Mg. In addition, Fe^{3+} was detected in some samples (5–10 mol% of total Fe); based on theoretical calculations of the EXAFS region this was thought to be located at the five-coordinated MgFe sites or the most distorted six-coordinated Al positions (depending on the sample studied).

EXPERIMENTAL METHODS

Seven samples with $X = 0.00$ to 0.52 (Table 1) were investigated in this study. Compositional data were obtained from the same crystals used for the crystal structure study (except for G8, which was lost during the preparation stage) with a CAMECA SX-50 electron microprobe operated in the wavelength-dispersion mode. Operating conditions were as follows: accelerating voltage, 15 kV; beam current, 10 nA; peak count time, 20 s; background count-time, 10 s; spot diameter (standards and specimen), 10 μm . Data reduction was done using the "PAP" $\phi(\rho Z)$ method (Pouchou and Pichoir 1985). For the elements considered, the following standards, X-ray lines, and crystals were used: P (apatite, $K\alpha$, PET), Si and Mg (diopside, $K\alpha$, TAP), Al (kyanite, $K\alpha$, PET), Cr (MgCr_2O_4 , $K\alpha$, LiF), Mn (MnSiO_3 , $K\alpha$, LiF), Fe (Fe_2SiO_4 , $K\alpha$, LiF), and Zn (gahnite, $K\alpha$, LiF). Formulas were calculated on the basis of six cations and nine O atoms per formula unit (Table 2).

Four of the samples (G1, G2, G4, and G8) were large enough to provide sufficient material for study by powder X-ray diffraction. Each sample was first ground into fine powder using an alumina mortar and smeared onto a glass slide. Data were collected over the range $10\text{--}80^\circ 2\theta$ with $\text{CoK}\alpha$ radiation on a standard Siemens (Bruker) D5000 Bragg-Brentano diffractometer equipped with a Vantec-1 strip detector, 0.6 mm (0.3°) divergence and antiscatter slits, and incident- and diffracted-beam Soller slits. The long fine-focus Co X-ray tube was operated at 35 kV and 40 mA, using a take-off angle of 6° . The X-ray diffraction pattern was analyzed using the ICDD (International Centre for Diffraction Data) database PDF-4 using search-match software supplied by Siemens (Bruker). Cell dimensions were determined using X-ray powder-diffraction data fitted with the LeBail method and the Rietveld program Topas 3.0 (Bruker AXS) in space group $Pbmn$. Starting values for cell dimensions were taken from Stephenson and Moore (1968), and the results are listed in Table 3.

For single-crystal X-ray diffraction measurements, the crystals were ground to approximate spheres using both an Enraf Nonius FR512 sphere grinder and a grinder made at UBC following the description in Cordero-Borboa (1985). Data were collected at C-HORSE (the Centre for Higher Order Structure Elucidation, in the Department of Chemistry at UBC) using a Bruker X8 APEX diffractometer with graphite-monochromated $\text{MoK}\alpha$ radiation and a CCD detector. Data were collected in a series of ϕ and ω scans in 0.50° oscillations with exposure times of 15.0 s. The crystal-to-detector distance was 40 mm. Data were collected and integrated using the Bruker SAINT software package and were corrected for absorption effects using the multi-scan technique (SADABS) and for Lorentz and polarization effects. All refinements were performed using the SHELXTL crystallographic software package of Bruker AXS. Neutral-atom scattering factors were taken from Cromer and Waber (1974). Anomalous dispersion effects were included in F_{calc} (Ibers and Hamilton 1964); the values for $\Delta f'$ and $\Delta f''$ were those of Creagh and McAuley (1992). The values for the mass attenuation coefficients were those of Creagh and Hubbell (1992).

The structures were refined in space group $Pbnm$ (a non-standard setting of $Pnma$, verified by the presence or absence of reflections in the full set of intensities) using the atom positions for grandidierite in Stephenson and Moore (1968). An extinction parameter was refined, and all atoms were refined anisotropically. Refinement was done using full-matrix least-squares in which the minimized function was $\sum w(F_o^2 - F_c^2)^2$ on F^2 . The weighting scheme was based on counting statistics.

The total occupancy factors of the three Al sites were refined to test the possibility of $(\text{Al},\text{Fe}^{3+})$ solid solution, as suggested by the electron microprobe compositions. The results ranged from 0.487(2) to 0.494(2) for Al1, 0.490(2) to 0.499(2) for Al2, and 0.488(2) to 0.498(2) for Al3, which would normally be indicative of a small degree of substitution. We then attempted to refine for Fe at the Al sites, but were unsuccessful, likely because the amounts of Fe (as indicated by the electron microprobe compositions) are so small. Accordingly, the occupancies of all three Al sites were fixed (at 1.0 Al atom each) in the final cycles of refinement.

To estimate the accuracy of unit-cell parameters obtained with our single-crystal diffractometer we also collected a data set from a single-crystal of "IUCr" ruby, for which Wong-Ng et al. (2001) give unit-cell dimensions of $a = 4.7608(3)$ and $c = 12.9957(9)$ Å.

Data collection and refinement parameters are summarized in Table 3, observed

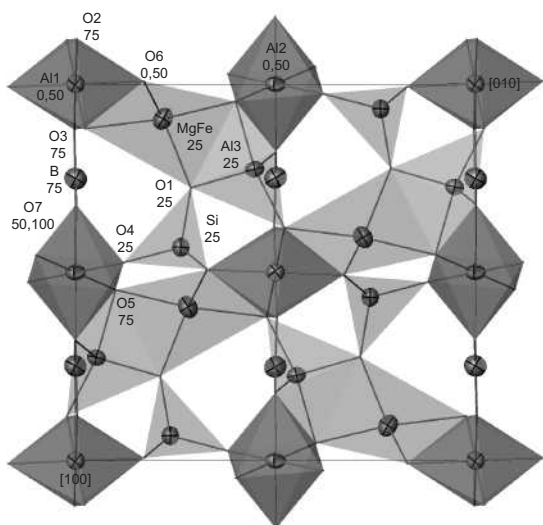


FIGURE 1. Projection of the crystal structure of grandidierite and ominelite onto (001). The atomic displacement ellipses represent 99% probability. The z coordinates $\times 100$ are given for each cation.

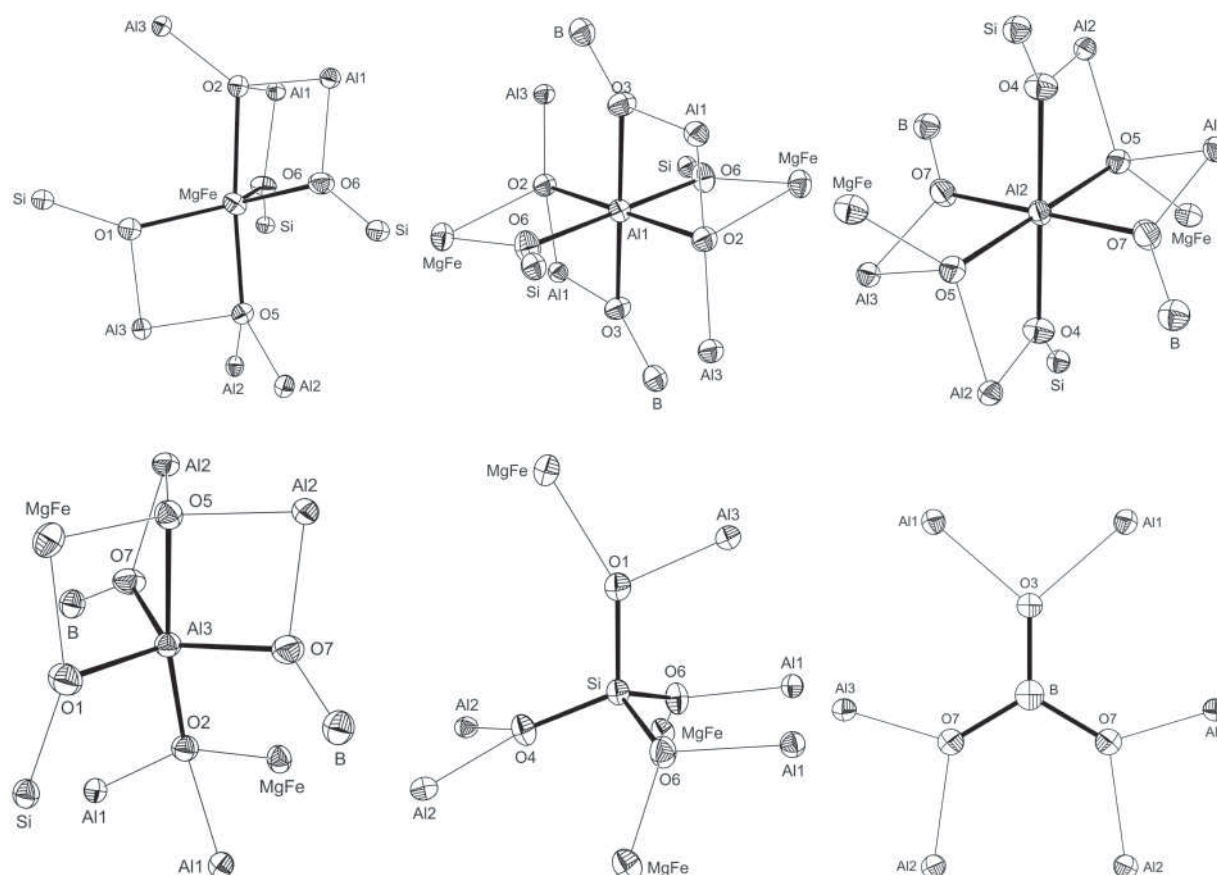


FIGURE 2. Coordination polyhedra for the cations in the grandidierite-ominelite structure. Orientations were chosen to give the best view of the atoms and bonds. The diagrams are in perspective with a view distance of 50 cm. The atomic displacement ellipsoids represent 90% probability.

TABLE 1. Sample information for grandidierite and ominelite

	G17	G8	G4	G12	G1	G2	G9
Locality	Madagascar	Long Lake, Larsemann Hills, Antarctica	Sahakondra, Ampamatoa, Madagascar	Zimbabwe	Karibe area, Zimbabwe	Andrahomana, Madagascar	Almgjotheii, Rogaland, Norway
Source	Royal Ontario Museum	H.-M. Braun	Harvard	Canadian Museum of Nature	Smithsonian	Mus. Nat. Hist. Naturelle	ESG
Sample number	32806	63	108118	80693	144869	102.149	Alm 8a
Color	transparent	turquoise	light blue	dark blue	green-blue	turquoise	medium blue
References		Stüwe et al. (1989), Carson et al. (1995), Grew et al. (1998b)		Grew et al. (1997)	Grew et al. (1997)	Grew et al. (1998a)	Grew et al. (1998a)

and calculated structure factors in Table 4¹, positional parameters in Table 5, displacement parameters in Table 6¹, bond lengths and angles in Table 7, polyhedral edges in Table 8¹, and polyhedral volumes and distortion parameters in Table 9¹.

RESULTS

Electron microprobe analyses

Average electron microprobe analyses (EMPA) of the crystals used in the structure refinement (SREF) study are given in Table 2. The electron microprobe compositions show a very low degree of substitutions other than Fe^{2+} for Mg. Manganese attains a maximum of 0.14 wt% MnO (~ 0.01 Mn apfu) in sample G12. Samples G8 and G1 contain up to 0.31 and 0.24 wt% P_2O_5 , respectively, corresponding to ~ 0.01 P apfu; G8 also shows up to 0.42 wt% Cr_2O_3 (0.02 Cr apfu). The significance of P and Cr is

unknown; presumably the former would substitute for Si at the Si position, and the latter for Al at one of the Al sites. Sample G9 contains up to 0.29 wt% ZnO (0.01 Zn apfu). The calculated

¹ Deposit item AM-07-021, Tables 4, 6, 8, and 9, (observed and calculated structure factors in Table 4; displacement parameters in Table 6; polyhedral edges in Table 8; and polyhedral volumes and distortion parameters in Table 9). Deposit items are available two ways: For a paper copy contact the Business Office of the Mineralogical Society of America (see inside front cover of recent issue) for price information. For an electronic copy visit the MSA web site at <http://www.minsocam.org>, go to the American Mineralogist Contents, find the table of contents for the specific volume/issue wanted, and then click on the deposit link there.

TABLE 2. Average electron-microprobe compositions of grandidierite and ominelite crystals used in the single-crystal X-ray diffraction study

	G17	G8	G4	G12	G1	G2	G9
<i>n</i>	7	4	4	5	4	4	3
P ₂ O ₅	bdl	0.24(5)	bdl	0.07(5)	0.19(6)	0.08(3)	bdl
SiO ₂	20.26(6)	19.88(4)	20.12(19)	19.77(9)	19.53(9)	19.49(10)	19.57(4)
B ₂ O ₃ *	11.91(2)	11.78(3)	11.84(3)	11.64(2)	11.57(3)	11.41(2)	11.33(3)
Al ₂ O ₃	52.01(20)	50.74(15)	51.65(27)	50.68(10)	50.18(10)	49.63(11)	48.93(3)
Cr ₂ O ₃	bdl	0.34(5)	bdl	bdl	bdl	bdl	bdl
Fe ₂ O ₃	1.03(5)	1.62(19)	1.35(41)	1.38(29)	1.62(11)	1.09(15)	1.21(45)
MgO	13.71(5)	11.99(8)	11.35(5)	10.02(7)	9.06(8)	7.30(3)	6.22(6)
MnO	bdl	bdl	0.06(3)	0.08(3)	0.08(2)	bdl	bdl
FeO	0.01(2)	2.81(23)	3.73(33)	5.78(29)	7.39(7)	10.36(15)	11.95(19)
ZnO	bdl	bdl	bdl	bdl	bdl	bdl	0.23(5)
Total	99.00(18)	99.46(27)	100.17(24)	99.45(18)	99.70(27)	99.48(22)	99.60(33)
P ⁵⁺	–	0.01(0)	–	0.00(0)	0.01(0)	0.00(0)	–
Si ⁴⁺	0.99(0)	0.98(0)	0.98(1)	0.98(0)	0.98(0)	0.99(0)	1.00(0)
B ³⁺	1.00	1.00	1.00	1.00	1.00	1.00	1.00
Al ³⁺	2.98(1)	2.94(0)	2.98(1)	2.97(0)	2.96(1)	2.97(1)	2.95(2)
Cr ³⁺	–	0.01(0)	–	–	–	–	–
Fe ³⁺	0.04(0)	0.06(1)	0.05(2)	0.05(1)	0.06(0)	0.04(1)	0.05(2)
Mg ²⁺	0.99(0)	0.88(0)	0.83(0)	0.74(1)	0.68(0)	0.55(0)	0.47(0)
Mn ²⁺	–	–	0.00(0)	0.00(0)	0.00(0)	–	–
Fe ²⁺	0.00(0)	0.12(1)	0.15(1)	0.24(1)	0.31(0)	0.44(1)	0.51(1)
Zn ²⁺	–	–	–	–	–	–	0.01(0)
<i>X</i> _{EMPA} †	0.00(0)	0.12(1)	0.16(1)	0.25(1)	0.32(0)	0.45(0)	0.52(1)
<i>X</i> _{SREF} ‡	0.024(1)	0.126(2)	0.184(4)	0.273(2)	0.336(2)	0.450(2)	0.522(2)

Notes: The G8 crystal was lost subsequent to SREF data collection; the analyses were obtained from a crystal from the same sample. Compositions were recalculated on the basis of 6 cations and 9 O apfu. Ti, Ca, Na, and K were sought but not detected. bdl = below detection limit (assumed to be 0.05 oxide wt%).

* Determined by stoichiometry.

† $X_{EMPA} = (\text{Fe}^{2+} + \text{Mn} + \text{Zn}) / (\text{Fe}^{2+} + \text{Mn} + \text{Zn} + \text{Mg})$.

‡ $X_{SREF} = \text{Fe} / (\text{Fe} + \text{Mg})$.

TABLE 3. Data measurement and refinement information for grandidierite and ominelite

	G17	G8	G4	G12	G1	G2	G9
<i>a</i> _{SCXRD} (Å)	10.3640(4)	10.3529(7)	10.3590(3)	10.3660(9)	10.3643(5)	10.3631(4)	10.3675(5)
<i>b</i> _{SCXRD} (Å)	10.9995(5)	10.9971(7)	11.0147(3)	11.0296(9)	11.0438(4)	11.0627(5)	11.0873(6)
<i>c</i> _{SCXRD} (Å)	5.7805(2)	5.7754(4)	5.7762(2)	5.7790(5)	5.7800(3)	5.7778(2)	5.7879(3)
<i>V</i> _{SCXRD} (Å ³)	658.98(6)	657.5(1)	659.07(4)	660.7(1)	661.58(7)	662.39(8)	665.30(8)
<i>a</i> _{PXRD} (Å)		10.3330(2)	10.3317(2)		10.3360(2)	10.3403(2)	
<i>b</i> _{PXRD} (Å)		10.9858(4)	10.9904(3)		11.0148(4)	11.0332(3)	
<i>c</i> _{PXRD} (Å)		5.7667(3)	5.7634(2)		5.7657(2)	5.7655(2)	
<i>V</i> _{PXRD} (Å ³)		654.62(4)	654.44(3)		656.41(3)	657.77(3)	
Space group	<i>Pbnm</i>						
Z	4	4	4	4	4	4	4
Crystal size (mm)	0.28 × 0.27 × 0.24	0.26 × 0.26 × 0.24	0.25 × 0.20 × 0.20	0.14 × 0.14 × 0.20	0.32 × 0.26 × 0.20	0.24 × 0.24 × 0.18	0.32 × 0.25 × 0.25
Radiation	MoKα						
Monochromator	graphite						
Total <i>F</i> _o	13314	16164	13534	13867	18782	17377	14875
Unique <i>F</i> _o	902	900	901	908	901	906	898
<i>F</i> _o > 4σ <i>F</i> _o	869	870	854	833	894	882	873
<i>R</i> _{int}	0.021(9)	0.03(1)	0.02(1)	0.03(1)	0.023(8)	0.023(9)	0.022(9)
L.s. parameters	87	87	87	87	87	87	87
<i>R</i> _i for <i>F</i> _o > 4σ <i>F</i> _o	0.0163	0.0166	0.0211	0.0205	0.0164	0.0141	0.0168
<i>R</i> _i , all unique <i>F</i> _o	0.0169	0.0172	0.0223	0.0225	0.0166	0.0145	0.0173
<i>wR</i> ₂	0.0502	0.0500	0.0584	0.0555	0.0485	0.0412	0.0466
<i>a</i>	0.0236	0.0237	0.0285	0.0276	0.0218	0.0233	0.0267
<i>b</i>	0.45	0.44	0.65	0.58	0.38	0.23	0.32
Goof (= <i>S</i>)	1.223	1.228	1.173	1.140	1.331	1.154	1.161

Note: $w = 1 / [\sigma^2(F_o) + (a \times P)^2 + b \times P]$ where $P = [\text{Max}(F_o, 0) + 2 \times F_o^2] / 3$.

* Single-crystal X-ray diffraction data.

† Powder X-ray diffraction data.

average Fe³⁺ compositions (0.04–0.06 apfu) are very low and the Fe atoms are presumably randomly distributed between all three Al sites, which is most likely why we were unable to refine for Fe at these sites in the SREF study.

Unit-cell parameters

Olesch and Seifert (1976) and Hiroi et al. (2002) showed that the unit-cell parameters of grandidierite and ominelite increase with $X = (\text{Fe}^{2+} + \text{Mn}) / (\text{Fe}^{2+} + \text{Mn} + \text{Mg})$, with *b* expanding the

most. The unit-cell parameters from this and previous studies are plotted against X_{EMPA} in Figure 3; the graphs show that *b* increases dramatically with increasing *X* (note that in this and subsequent figures the value of *X* used for ominelite is that of Yokoyama, 0.908, as listed in Hiroi et al. 2002). The amounts of expansion from $X = 0$ to $X = 1$, obtained from the regression equation calculated from our single-crystal data, is 0.18 Å (corresponding to a percentage increase of 1.6%). In contrast to *b* the *a* and *c* parameters show considerable scatter from $X = 0$ –1.

TABLE 5. Atomic parameters for grandidierite and ominelite

		G17	G8	G4	G12	G1	G2	G9
MgFe	x	0.09183(6)	0.09262(5)	0.09293(6)	0.09348(5)	0.09387(4)	0.09438(3)	0.09462(3)
	y	0.21910(5)	0.21906(5)	0.21903(5)	0.21897(5)	0.21896(4)	0.21894(3)	0.21896(3)
	z	1/4	1/4	1/4	1/4	1/4	1/4	1/4
Occ.	Mg	0.488(1)	0.437(1)	0.409(2)	0.363(2)	0.333(1)	0.275(1)	0.239(1)
	Fe	0.012(1)	0.063(1)	0.091(2)	0.137(2)	0.167(1)	0.225(1)	0.261(1)
Al1	x	0	0	0	0	0	0	0
	y	0	0	0	0	0	0	0
	z	0	0	0	0	0	0	0
Al2	x	1/2	1/2	1/2	1/2	1/2	1/2	1/2
	y	0	0	0	0	0	0	0
	z	0	0	0	0	0	0	0
Al3	x	0.22634(5)	0.22643(5)	0.22643(6)	0.22641(6)	0.22643(5)	0.22648(4)	0.22649(5)
	y	0.44792(4)	0.44799(4)	0.44795(6)	0.44796(5)	0.44807(4)	0.44810(4)	0.44811(4)
	z	1/4	1/4	1/4	1/4	1/4	1/4	1/4
Si	x	0.43356(5)	0.43370(5)	0.43377(6)	0.43394(5)	0.43406(5)	0.43423(4)	0.43431(5)
	y	0.26330(4)	0.26325(4)	0.26334(5)	0.26340(5)	0.26340(4)	0.26343(3)	0.26345(4)
	z	1/4	1/4	1/4	1/4	1/4	1/4	1/4
B	x	0.2512(2)	0.2512(2)	0.2512(2)	0.2511(2)	0.2512(2)	0.2512(2)	0.2510(2)
	y	0.0003(2)	0.0004(2)	0.0004(2)	0.0002(2)	0.0003(2)	0.0002(1)	0.0003(2)
	z	3/4	3/4	3/4	3/4	3/4	3/4	3/4
O1	x	0.2750(1)	0.2756(1)	0.2755(1)	0.2758(1)	0.2761(1)	0.2763(1)	0.2765(1)
	y	0.2882(1)	0.2883(1)	0.2888(1)	0.2892(1)	0.2891(1)	0.28964(9)	0.2898(1)
	z	1/4	1/4	1/4	1/4	1/4	1/4	1/4
O2	x	0.1186(1)	0.1183(1)	0.1184(1)	0.1183(1)	0.11818(9)	0.1182(1)	0.1181(1)
	y	0.0224(1)	0.0222(1)	0.0216(1)	0.0214(1)	0.0214(1)	0.02087(9)	0.0205(1)
	z	1/4	1/4	1/4	1/4	1/4	1/4	1/4
O3	x	0.1210(1)	0.1211(1)	0.1212(2)	0.1209(1)	0.1210(1)	0.1210(1)	0.1211(1)
	y	-0.0035(1)	-0.0033(1)	-0.0036(1)	-0.0037(1)	-0.0036(1)	-0.00373(8)	-0.0037(1)
	z	3/4	3/4	3/4	3/4	3/4	3/4	3/4
O4	x	0.4738(1)	0.4738(1)	0.4739(2)	0.4738(1)	0.4739(1)	0.4738(1)	0.4740(1)
	y	0.1199(1)	0.1202(1)	0.1201(1)	0.1203(1)	0.1205(1)	0.12070(9)	0.1208(1)
	z	1/4	1/4	1/4	1/4	1/4	1/4	1/4
O5	x	0.5465(1)	0.5465(1)	0.5463(1)	0.5464(1)	0.5465(1)	0.54644(9)	0.5464(1)
	y	0.1002(1)	0.0999(1)	0.0997(1)	0.0992(1)	0.0988(1)	0.09836(9)	0.0981(1)
	z	3/4	3/4	3/4	3/4	3/4	3/4	3/4
O6	x	-0.00731(8)	-0.00755(8)	-0.00720(9)	-0.00728(9)	-0.00724(8)	-0.00717(6)	-0.00700(8)
	y	0.17099(8)	0.17090(8)	0.1708(1)	0.1707(1)	0.17053(8)	0.17035(7)	0.17034(8)
	z	-0.0227(2)	-0.0227(2)	-0.0225(2)	-0.0228(2)	-0.0228(2)	-0.0231(1)	-0.0231(1)
O7	x	0.18068(9)	0.18059(9)	0.1807(1)	0.1807(1)	0.18054(9)	0.18067(7)	0.18070(8)
	y	0.50112(7)	0.50118(7)	0.50117(9)	0.50113(9)	0.50112(7)	0.50109(6)	0.50115(7)
	z	-0.0452(2)	-0.0452(2)	-0.0453(2)	-0.0455(2)	-0.0452(2)	-0.0454(1)	-0.0453(2)

The unit-cell volume increases by approximately 13 \AA^3 (1.9%) over the same range.

Structural changes with Fe for Mg substitution

The most "significant" changes (arbitrarily chosen to be those $>2\%$) resulting from Fe for Mg substitution at the MgFe site are as follows: (1) increase in the volume of the $(\text{Mg}, \text{Fe}^{2+})\text{O}_5$ polyhedron (5.0% change; Fig. 4); (2) expansion of the M–O5 bond distance (4.4%; Fig. 5a); (3) expansion of the O1–O2 edge (3.6%; Fig. 6a); (4) opening of the O1–M–O2 angle (3.2%; Fig. 7); (5) increase in the length of the O6–O5a ($\times 2$) edges (2.8%; Fig. 6b); (6) lengthening of the M–O2 bond distance (2.8%; Fig. 5b); (7) decrease in the O6–M–O6b angle (-2.1% ; Fig. 7); (8) increase in the M–O6 ($\times 2$) bond distances (2.0%; Fig. 5c); and (9) opening of the O1–Al3–O5a angle (2.0%; Fig. 8).

DISCUSSION

Unit-cell parameters

Figure 3 also shows that the unit-cell parameters from the single-crystal studies are displaced above (our data) and below (previous studies) the trends established by parameters from powder experiments (both our study and previous studies). It is possible that the unit-cell parameters derived from powder

diffraction data (especially when obtained using the Rietveld method and an internal standard) are more accurate than those obtained from single-crystal data. In addition, point detectors may be preferable to CCDs for accurate unit-cell determinations (G.A. Lager, pers. comm.). However, the unit-cell dimensions obtained from the "IUCr" ruby [$a = 4.7642(6)$ and $c = 13.010(2)$ \AA], although somewhat higher than the published values (by 0.07 and 0.11%, respectively), are not displaced to the same degree as the grandidierite and ominelite cell parameters.

Figure 3 also shows that, as previously noted by Hiroi et al. (2002), the a dimension for the synthetic samples (from powder data) is much longer than expected (and similar to our single-crystal results), and b and c are noticeably shorter. We do not know the reason for this, but suggest that it might be due to Mg–Al disorder in the synthetic samples. Mg–Al disorder might also be invoked to explain the overall scattering of the a and c values, as might the presence of structural vacancies (perhaps balanced by $\text{Fe}^{3+}/\text{Fe}^{2+}$) and substitutions (Be, B, etc.) at the tetrahedral site.

Figure 3 also shows that the unit-cell parameters of ominelite from the single-crystal study of Hiroi et al. (2002) are considerably offset from the trends established by the single-crystal data from this study. However in most cases the bond distances and angles and other geometrical parameters correspond quite well.

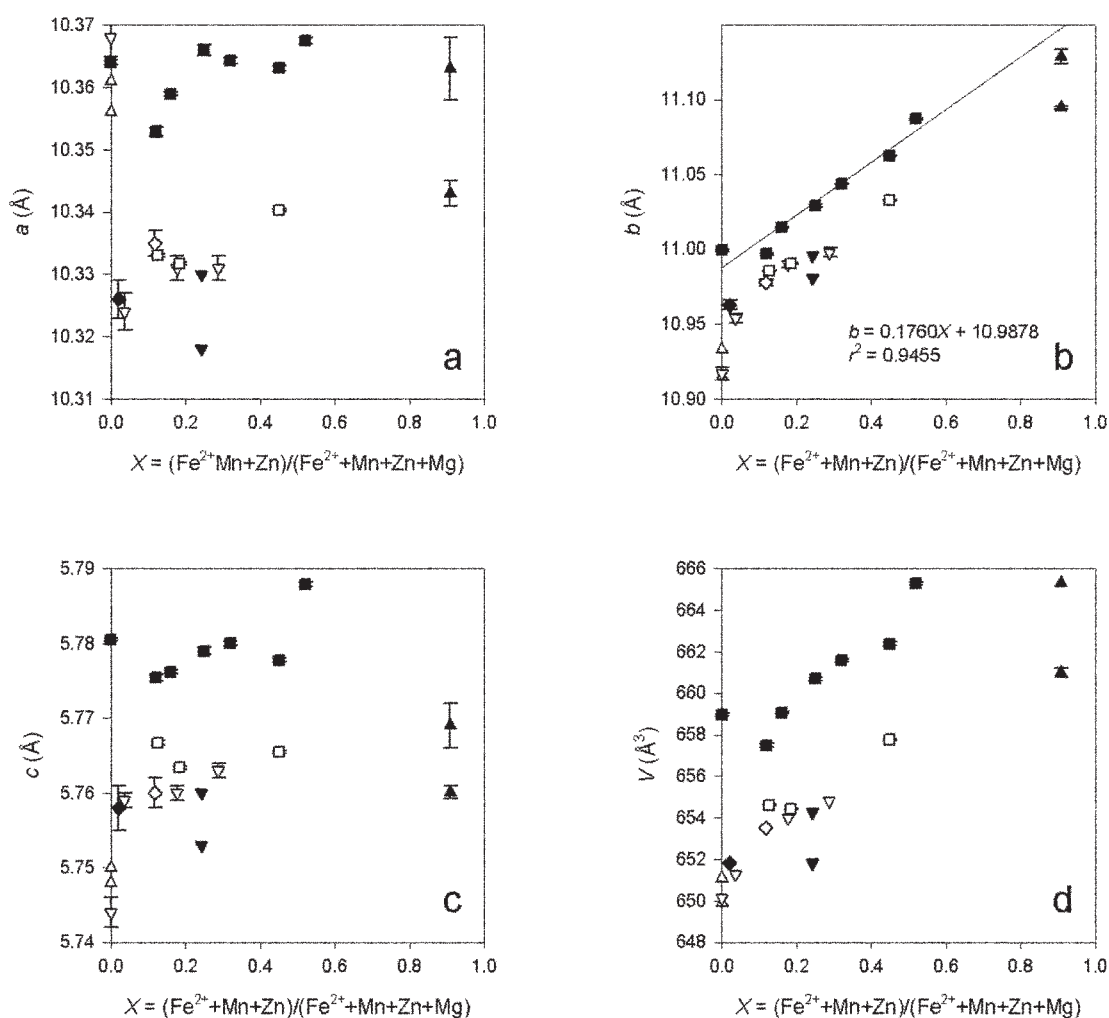


FIGURE 3. $(\text{Fe}^{2+} + \text{Mn} + \text{Zn})/(\text{Fe}^{2+} + \text{Mn} + \text{Zn} + \text{Mg})$ vs. (a) a , (b) b , (c) c , (d) V for grandidierite and ominelite. Filled squares = this study, single-crystal X-ray diffraction; open squares = this study, powder X-ray diffraction; filled upward-pointing triangles = Hiroi et al. (2002); open upward-pointing triangles = Heide (1992); filled downward-pointing triangles = Qiu et al. (1990) for X , Tan and Lee (1988) for cell parameters; open downward-pointing triangles = Olesch and Seifert (1976); filled diamond = von Knorring et al. (1969); open diamond = McKie (1965). The Heide (1992) and Olesch and Seifert (1976) $X = 0$ data is from synthetic samples. The lowest point on each graph corresponding to Hiroi et al. (2002) and Qiu et al. (1990)/Tan and Lee (1988) are from single-crystal X-ray diffraction experiments; the rest of the points from the literature are from powder data.

In those cases where the correspondence is less than ideal it may be due to some unknown characteristic of their crystal but is more likely due to the fact that the data was collected with different instruments. It is unfortunate that we were unable to obtain the sample studied by Hiroi et al. (2002) or any other crystals with $X > 0.52$.

Geometric effects

Given the difference in diameter of almost 0.1 \AA it is not surprising that Fe^{2+} for Mg substitution at the MgFe site in members of the grandidierite-ominelite series leads to noticeable changes in the crystal structure. However, these are influenced by the following factors: (1) all of the atoms except O6 and O7 are at special positions (Al1 at $0,0,0$; Al2 at $1/2,0,0$; MgFe , Al3, O1, O2, and O4 at $x,y,1/4$; B, O3, and O5 at $0,0,3/4$) where z (at least) is constrained. Therefore, changes to atom positions are mostly

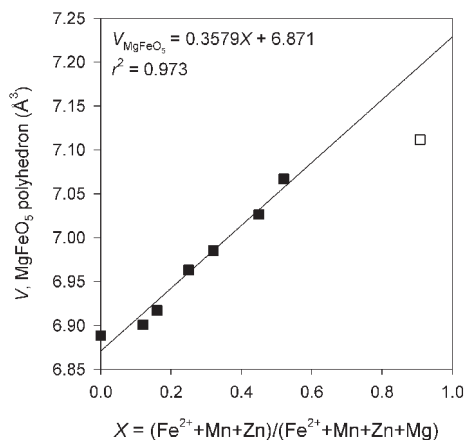


FIGURE 4. $(\text{Fe}^{2+} + \text{Mn} + \text{Zn})/(\text{Fe}^{2+} + \text{Mn} + \text{Zn} + \text{Mg})$ vs. volume of the $(\text{Mg}, \text{Fe}^{2+})\text{O}_3$ polyhedron in grandidierite and ominelite.

TABLE 7. Interatomic distances (Å) and angles (°) for grandidierite and ominelite

		G17	G8	G4	G12	G1	G2	G9
M-O6	× 2	1.9545(9)	1.9588(9)	1.959(1)	1.964(1)	1.9675(9)	1.9715(7)	1.9745(8)
-O5a		2.0426(1)	2.048(1)	2.054(2)	2.064(2)	2.072(1)	2.081(1)	2.089(1)
-O1		2.045(1)	2.042(1)	2.041(1)	2.043(2)	2.041(1)	2.041(1)	2.043(1)
-O2		2.182(1)	2.182(1)	2.191(2)	2.194(2)	2.197(1)	2.205(1)	2.214(1)
<M-O>		2.036	2.038	2.041	2.046	2.049	2.054	2.059
O6-M-O6b		107.50(6)	107.05(5)	106.97(6)	106.71(6)	106.55(5)	106.35(4)	106.35(5)
-O1	× 2	126.06(3)	126.31(3)	126.36(3)	126.50(3)	126.58(3)	126.69(2)	126.69(2)
-O5a	× 2	98.19(4)	98.01(4)	98.01(4)	97.90(4)	97.91(4)	97.90(3)	97.90(3)
-O2	× 2	78.37(4)	78.23(4)	78.14(4)	78.08(4)	77.94(3)	77.80(3)	77.72(3)
O5a-M-O1		81.49(5)	81.60(5)	81.46(6)	81.40(6)	81.41(5)	81.28(4)	81.22(5)
O1-M-O2		104.51(5)	104.92(5)	105.21(6)	105.55(6)	105.73(5)	106.10(4)	106.30(5)
<O-M-O>		99.86	99.85	99.85	99.85	99.84	99.83	99.83
Al1-O6	× 2	1.8869(9)	1.8855(9)	1.887(1)	1.889(1)	1.8894(9)	1.8906(7)	1.8947(9)
-O2	× 2	1.9132(8)	1.9086(8)	1.910(1)	1.909(1)	1.9089(8)	1.9078(6)	1.9091(8)
-O3c	× 2	1.9141(8)	1.9123(8)	1.914(1)	1.913(1)	1.9136(8)	1.9134(7)	1.9162(8)
<Al1-O>		1.905	1.902	1.904	1.904	1.904	1.904	1.907
O6-Al1-O2	× 2	87.14(4)	87.25(5)	87.32(5)	87.43(5)	87.43(5)	87.60(4)	87.68(4)
-O2d	× 2	92.86(4)	92.75(5)	92.68(5)	92.57(5)	92.57(5)	92.40(4)	92.32(4)
-O3c	× 2	89.66(4)	89.65(4)	89.69(5)	89.71(5)	89.67(4)	89.65(3)	89.62(4)
-O3e	× 2	90.34(4)	90.36(4)	90.31(5)	90.29(5)	90.33(4)	90.35(3)	90.38(4)
O2-Al1-O3c	× 2	98.73(4)	98.81(4)	98.73(5)	98.78(5)	98.85(4)	98.82(3)	98.89(4)
-O3e	× 2	81.27(4)	81.19(4)	81.27(5)	81.22(5)	81.15(4)	81.18(3)	81.11(4)
<O-Al1-O>		90.00	90.00	90.00	90.00	90.00	90.00	90.00
Al2-O5c	× 2	1.8801(7)	1.8768(8)	1.8767(9)	1.8744(9)	1.8736(8)	1.8714(6)	1.8732(7)
-O7f	× 2	1.8907(9)	1.8878(9)	1.890(1)	1.891(1)	1.8893(9)	1.8906(8)	1.8916(9)
-O4	× 2	1.9750(8)	1.9765(8)	1.977(1)	1.980(1)	1.9831(8)	1.9857(7)	1.9903(8)
<Al2-O>		1.915	1.914	1.915	1.915	1.915	1.916	1.918
O5c-Al2-O7f	× 2	81.74(4)	81.77(4)	81.79(5)	81.76(5)	81.72(4)	81.72(4)	81.74(4)
-O7g	× 2	98.27(4)	98.23(4)	98.21(5)	98.24(5)	98.28(4)	98.28(4)	98.26(4)
-O4	× 2	101.90(4)	101.86(4)	101.86(5)	101.89(5)	101.90(4)	101.87(3)	101.86(4)
-O4h	× 2	78.10(4)	78.13(4)	78.14(5)	78.11(5)	78.10(4)	78.13(3)	78.14(4)
O7f-Al2-O4	× 2	92.25(4)	92.26(5)	92.24(5)	92.24(5)	92.24(5)	92.23(4)	92.19(4)
-O4h	× 2	87.75(4)	87.74(5)	87.76(5)	87.76(5)	87.76(5)	87.77(4)	87.81(4)
<O-Al2-O>		90.00	90.00	90.00	90.00	90.00	90.00	90.00
Al3-O2i		1.804(1)	1.803(1)	1.801(2)	1.802(2)	1.803(1)	1.800(1)	1.800(1)
-O1		1.828(1)	1.828(1)	1.825(2)	1.825(2)	1.829(1)	1.828(1)	1.830(1)
-O7b	× 2	1.8649(9)	1.864(1)	1.865(1)	1.866(1)	1.866(1)	1.8658(8)	1.8686(9)
-O5a		1.938(1)	1.936(1)	1.938(2)	1.937(2)	1.936(1)	1.935(1)	1.936(1)
<Al3-O>		1.860	1.859	1.859	1.859	1.860	1.859	1.861
O2i-Al3-O1		100.99(6)	100.73(6)	100.62(7)	100.40(7)	100.35(6)	100.15(5)	100.01(6)
-O7	× 2	94.79(4)	94.88(4)	94.88(4)	94.92(4)	94.98(3)	95.00(3)	95.00(3)
O1-Al3-O7b	× 2	111.82(3)	111.86(3)	111.88(4)	111.90(4)	111.90(3)	111.92(2)	111.95(3)
-O5a		90.17(6)	90.39(6)	90.44(7)	90.74(7)	90.82(6)	91.02(5)	91.10(5)
O7b-Al3-O7		132.40(6)	132.33(6)	132.31(7)	132.31(7)	132.28(6)	132.31(5)	132.29(6)
-O5a	× 2	80.89(3)	80.81(3)	80.83(4)	80.77(4)	80.70(3)	80.69(3)	80.70(3)
<O-Al3-O>		99.84	99.84	9.84	99.85	99.85	99.86	99.86
Si-O6j	× 2	1.6202(9)	1.6178(9)	1.621(1)	1.619(1)	1.6206(9)	1.6197(7)	1.6260(9)
-O4		1.632(1)	1.627(1)	1.632(2)	1.632(2)	1.631(1)	1.631(1)	1.634(1)
-O1		1.666(1)	1.660(1)	1.664(2)	1.663(2)	1.662(1)	1.662(1)	1.662(1)
<Si-O>		1.635	1.631	1.635	1.633	1.634	1.633	1.637
O6j-Si-O6f		108.41(7)	108.46(7)	108.33(8)	108.30(8)	108.23(7)	108.04(6)	108.05(6)
-O4	× 2	109.55(4)	109.68(4)	109.69(5)	109.81(5)	109.92(4)	110.10(4)	110.09(4)
-O1	× 2	107.44(4)	107.24(4)	107.23(5)	107.10(5)	107.03(4)	106.87(3)	106.83(4)
O4-Si-O1		114.28(7)	114.35(7)	114.47(8)	114.51(8)	114.49(7)	114.60(5)	114.70(6)
<O-Si-O>		109.45	109.44	109.44	109.44	109.44	109.43	109.43
B-O3		1.350(2)	1.348(2)	1.348(3)	1.350(3)	1.350(2)	1.350(2)	1.348(2)
-O7k	× 2	1.379(1)	1.377(1)	1.377(2)	1.377(2)	1.379(1)	1.377(1)	1.381(1)
<B-O>		1.369	1.367	1.367	1.368	1.369	1.368	1.370
O3-B-O7k	× 2	120.80(8)	120.83(8)	120.8(1)	120.92(9)	120.87(8)	120.85(7)	120.86(8)
O7k-B-O7l		118.4(2)	118.3(2)	118.4(2)	118.2(2)	118.3(2)	118.3(1)	118.3(2)
<O-B-O>		120.0	120.0	120.0	120.0	120.0	120.0	120.0

Notes: M = MgFe; a = $x - \frac{1}{2}, -y + \frac{1}{2}, -z + 1$; b = $x, y, -z + \frac{1}{2}$; c = $x, y, z - 1$; d = $-x, -y, -z + 1$; e = $-x, -y, -z + 1$; f = $x + \frac{1}{2}, -y + \frac{1}{2}, -z$; g = $-x + \frac{1}{2}, y - \frac{1}{2}, z$; h = $-x + 1, -y, -z$; i = $-x + \frac{1}{2}, y + \frac{1}{2}, z$; j = $x + \frac{1}{2}, -y + \frac{1}{2}, z + \frac{1}{2}$; k = $-x + \frac{1}{2}, y - \frac{1}{2}, -z + \frac{1}{2}$; l = $-x + \frac{1}{2}, y - \frac{1}{2}, z + 1$.

limited to the **a-b** plane. (2) B and Si are small, relatively highly charged cations, and thus would be expected to form strong bonds to O atoms that would resist change in length.

Olesch and Seifert (1976) and Hiroi et al. (2002) suggested that the increase in unit-cell dimensions with increasing X is due to expansion of the M-O2 and -O5 bond lengths with X . Our results show that not only M-O2 and -O5 but also M-O6 increases with increasing substitution of Fe. Only M-O1 is unaffected by Fe substitution. The O atom at O1 is also bonded to an Al atom at

Al3 and an Si atom at the Si site. The Al3-O1 and Si-O1 distances also remain constant (within error) with increasing X , perhaps because the O1 atom is prevented from moving by the relatively strong Si-O bond. The two M-O distances that increase the most are the two (M-O5 and -O2) that are approximately perpendicular to the M-O1 bond. The two M-O6 bond lengths do not expand as much as the M-O5 and -O2 distances, likely because the O atoms at the O6 sites also form bonds with Si atoms. The two short Al1-O6 bond distances increase only slightly with X , likely

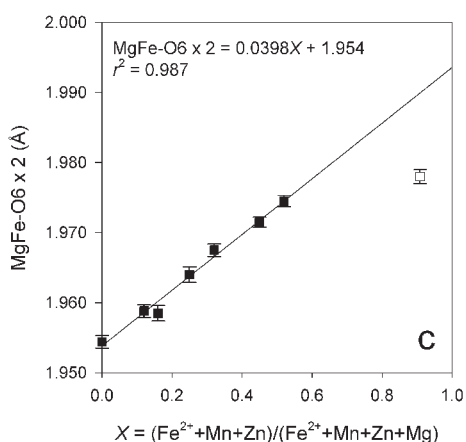
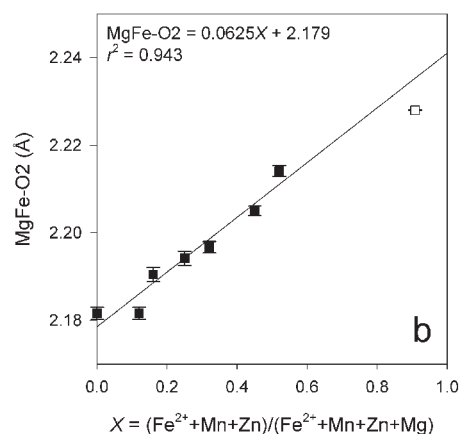
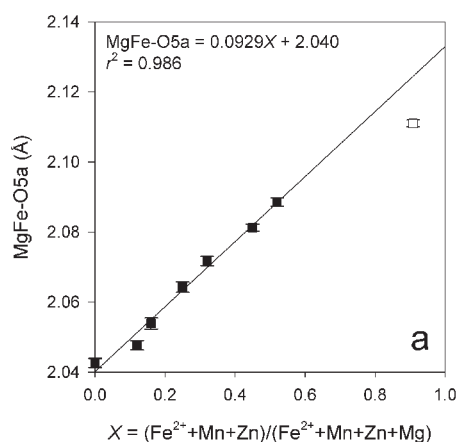


FIGURE 5. $(\text{Fe}^{2+} + \text{Mn} + \text{Zn})/(\text{Fe}^{2+} + \text{Mn} + \text{Zn} + \text{Mg})$ vs. (a) M (= MgFe)-O5a, (b) M-O2, (c) M-O6 \times 2 for grandidierite and ominelite.

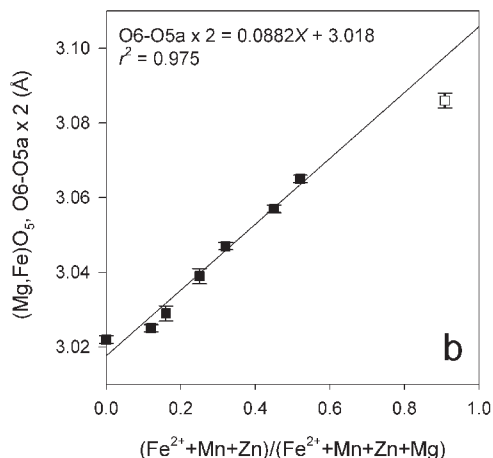
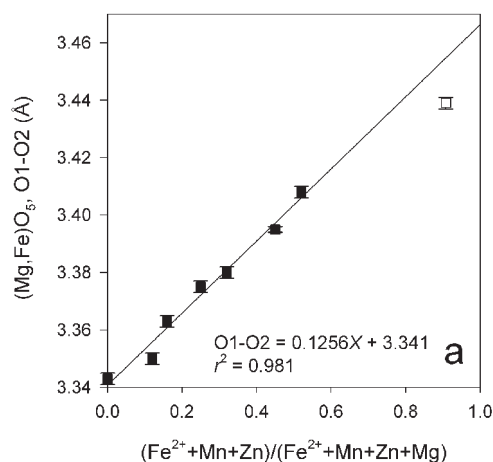


FIGURE 6. $(\text{Fe}^{2+} + \text{Mn} + \text{Zn})/(\text{Fe}^{2+} + \text{Mn} + \text{Zn} + \text{Mg})$ vs. $(\text{Mg,Fe}^{2+})\text{O}_5$ polyhedral edges: (a) O1-O2; (b) O6-O5a \times 2 for grandidierite and ominelite.

because the Al1 site is constrained at the origin, but probably also because of the strong Si-O6 bonds.

The Al2-O5 distance shows the greatest decrease with X , probably in response to the increase in M-O5 (the O atom at the O5 site is bonded to Al atoms at two Al2 and one Al3 sites, and to the atom at one MgFe position). The Al3-O5 distance shows only a minor decrease.

As suggested above, it is not surprising that the lengths of the relatively strong Si-O bonds show no apparent change with X . Instead, the SiO_4 tetrahedra react to Fe for Mg substitution at the MgFe site by changing O-Si-O angles such that the tetrahedral angle variance and mean tetrahedral quadratic elongation increase. This is not surprising given that three of the four O atoms coordinating each Si atom (O1 and O6 \times 2) also form bonds to atoms at three different MgFe sites. The BO_3 triangles appear to behave as relatively invariant units in the crystal structure; this is also not surprising given that none of the O atoms coordinating each B atom form bonds to atoms at MgFe sites.

Effect of other substituents

Although the concentrations of substituents other than Fe^{2+} in our samples is very low, it is interesting to speculate on the effects of other reported substitutions on the structures of grandidierite and ominelite. For example, Hiroi et al. (2002) reported

up to 0.77 wt% MnO (~ 0.04 Mn apfu) in their ominelite sample, and according to Shannon (1976) the ionic radius of Mn^{2+} (high spin) is 0.75 Å, so substitution of Mn^{2+} at the MgFe site would

be expected to cause more distortion than an equivalent amount of Fe^{2+} . On the other hand, the ionic radius of ${}^{\vee}\text{Zn}$, given by Shannon (1976) as 0.68 Å, is only slightly larger than that of Mg and would likely have little effect. The ionic radii of ${}^{\vee}\text{Al}$ and ${}^{\vee}\text{Al}$ were given by Shannon (1976) as 0.48 and 0.535 Å, respectively, hence the presence of Cr (with an ionic radius of 0.615 Å for ${}^{\vee}\text{Cr}^{3+}$; Shannon 1976) at any of the Al sites would be expected to increase the size of the coordination sphere. On the other hand, the substitution of P^{5+} for Si at the Si sites, with the respective ionic radii of 0.17 and 0.26 Å (Shannon 1976), would be expected to decrease the bond distances, and of course there would be a charge imbalance to deal with.

Ionic radius of ${}^{\vee}\text{Fe}^{2+}$

Shannon (1976) reported an “ionic radius” of 0.66 Å for ${}^{\vee}\text{Mg}$ but no value was given for five-coordinated Fe^{2+} . However, the average of the radii of ${}^{\text{IV}}\text{Fe}^{2+}$ (0.63 Å) and ${}^{\text{VI}}\text{Fe}^{2+}$ (0.78 Å) (both high spin) is 0.71 Å. The average M-O distances determined from the regression equations (with M-O1 = 2.04 Å) in Figure 4 are 2.033 Å for $X = 0$ and 2.080 Å for $X = 1$. If the difference (0.047 Å) is added to the ionic radius of ${}^{\vee}\text{Mg}$ the result is 0.70 Å for ${}^{\vee}\text{Fe}^{2+}$, in good accordance with the Shannon (1976) data. These ionic radii differ from that of ${}^{\vee}\text{Mg}$ by ~7% which is much lower than the generally accepted upper limit for solid solution of 15%, but similar to the difference of ~8% reported for ${}^{\vee}\text{Mg}$ vs. ${}^{\vee}\text{Fe}^{2+}$ (Oberti 2001).

${}^{\vee}\text{Fe}$ in minerals

Ominelite is one of the few minerals in which Fe^{2+} is the dominant cation in a fivefold-coordinated site; other examples are graffonite, joaquinite, and vesuvianite. Kostiner and Rea (1974) studied the crystal structure of synthetic end-member graffonite and showed that there is one octahedron and two five-coordinated polyhedra that lie somewhere between a trigonal bipyramid and a tetragonal pyramid. They obtained average ${}^{\vee}\text{Fe}^{2+}$ -O bond distances of 2.134 and 2.101 Å. Dowty (1975) showed that the structure of monoclinic joaquinite, ideal formula $\text{NaFe}^{2+}\text{Ba}_2\text{REE}_2\text{Ti}_2\text{Si}_8\text{O}_{28}\text{OH}\cdot\text{H}_2\text{O}$, contains a trigonal dipyrmaid with composition $\text{Fe}^{2+}\text{O}_4(\text{OH})$ and an average bond distance of 2.10 Å.

The Y1 site in vesuvianite is coordinated by five anions that form a tetragonal pyramid (Groat et al. 1992). However, the site generally contains more than one element, and the substitutions and order/disorder in the vesuvianite structure make it difficult to say anything conclusive about Fe in this coordination.

As noted by Stephenson and Moore (1968), the degree of distortion of the $(\text{Mg},\text{Fe}^{2+})\text{O}_5$ polyhedron of the ominelite-grandidierite series can be estimated from the O2-M-O5a angle (which is 180° for a perfect trigonal bipyramid). A linear regression fit to the points in Figure 9 shows that this angle decreases from 173.9° for $X = 0$ to 171.0° for $X = 1$. The apparent rarity of ${}^{\vee}\text{Fe}$ in minerals is likely a function of the polyhedral distortion that is required to maintain this coordination as opposed to an octahedral coordination, especially for Fe^{2+} .

ACKNOWLEDGMENTS

The authors thank B. Patrick, A.E. Lam, and M. Raudsepp for help with data collection and J.G. Liou for a translation of Tan and Lee (1988). The manuscript was improved by comments from A. Liebscher, S. Matsubara, P. Bonazzi, and G.A. Lager. Financial support was provided by the Natural Sciences and Engineering Research Council of Canada in the form of a Discovery Grant to LAG. The equipment in C-HORSE was purchased with a grant from the Canadian Foundation for Innovation.

REFERENCES CITED

- Blass, G. and Graf, H.-W. (1994) Über neue Mineralien vom Bellerberg, Eifel. *Mineralien Welt*, 5, 53–55.
- Carson, C.J., Dirks, P.H.G.M., and Hand, M. (1995) Stable coexistence of grandidierite and kornerupine during medium pressure granulite facies metamorphism. *Mineralogical Magazine*, 59, 327–339.
- Cordero-Borboa, A.E. (1985) An improved grinder for single crystal X-ray diffraction work. *Journal of Physics E: Scientific Instruments*, 18, 393–395.
- Creagh, D.C. and Hubbell, J.H. (1992) Table 4.2.4.3. In A.J.C. Wilson, Ed., *International Tables for Crystallography*, Vol. C, p. 200–206. Kluwer Academic Publishers, Boston.
- Creagh, D.C. and McAuley, W.J. (1992) Table 4.2.6.8. In A.J.C. Wilson, Ed., *International Tables for Crystallography*, Vol. C, p. 219–222. Kluwer Academic Publishers, Boston.
- Cromer, D.T. and Waber, J.T. (1974) *International Tables for X-ray Crystallography*, Vol. IV. The Kynoch Press, Birmingham, U.K.
- Dowty, E. (1975) Crystal structure of joaquinite. *American Mineralogist*, 60, 872–878.
- Farges, F. (2001) Crystal chemistry of iron in natural grandidierite: an X-ray absorption fine-structure spectroscopy study. *Physics and Chemistry of Minerals*, 28, 619–629.
- Grant, J.A. and Frost, B.R. (1990) Contact metamorphism and partial melting of pelitic rocks in the aureole of the Laramie anorthosite complex, Morton Pass, Wyoming. *American Journal of Science*, 290, 425–472.
- Greenfield, J.E., Clarke, G.L., and White, R.W. (1998) A sequence of partial melting reactions at Mt. Stafford, central Australia. *Journal of Metamorphic Geology*, 16, 363–378.
- Grew, E.S. (1996) Borosilicates (exclusive of tourmaline) and boron in rock-forming minerals in metamorphic environments. In L.M. Anovitz and E.S. Grew, Eds., *Boron: Mineralogy, Petrology and Geochemistry*, 33, p. 387–502. *Reviews in Mineralogy*, Mineralogical Society of America, Chantilly, Virginia.
- Grew, E.S., Yates, M.G., Shearer, C.K., and Wiedenbeck, M. (1997) Werdingite from the Urungwe district, Zimbabwe. *Mineralogical Magazine*, 61, 713–718.
- Grew, E.S., Yates, M.G., Huijsmans, J.P.P., McGee, J.J., Shearer, C.K., Wiedenbeck, M., and Rouse, R.C. (1998a) Werdingite, a borosilicate new to granitic pegmatites. *Canadian Mineralogist*, 36, 399–414.
- Grew, E.S., McGee, J.J., Yates, M.G., Peacor, D.R., Rouse, R.C., Huijsmans, J.P.P., Shearer, C.K., Wiedenbeck, M., Thost, D.E., and Su, S.-C. (1998b) Boralsilite ($\text{Al}_4\text{B}_2\text{Si}_2\text{O}_7$): a new mineral related to sillimanite in pegmatites from granulite-facies rocks. *American Mineralogist*, 83, 638–651.
- Groat, L.A., Hawthorne, F.C., and Ercit, T.S. (1992) The chemistry of vesuvianite. *Canadian Mineralogist*, 30, 19–48.
- Heide, M. (1992) *Synthese und Stabilität von Grandidierit, MgAl₃BSiO₉*. Diplomarbeit, Ruhr-Universität Bochum, 90 p.
- Hiroi, Y., Motoyoshi, Y., Peacor, D.R., Rouse, R.C., Matsubara, S., Yokoyama, K., Miyawaki, R., McGee, J.J., Su, S.C., Hokada, T., Furukawa, N., and Shibusaki, H. (2002) Ominelite, $(\text{Fe},\text{Mg})\text{Al}_3\text{BSiO}_9$ (Fe^{2+} analogue of grandidierite), a new mineral from porphyritic granite in Japan. *American Mineralogist*, 87, 160–170.
- Huijsmans, J.P.P., Barton, M., and van Bergen, M.J. (1982) A pegmatite containing Fe-rich grandidierite, Ti-rich dumortierite and tourmaline from the Precambrian, high-grade metamorphic complex of Rogaland, S.W. Norway. *Neues Jahrbuch für Mineralogie Abhandlungen*, 143, 249–261.
- Ibers, J.A. and Hamilton, W.C. (1964) Dispersion corrections and crystal structure refinements. *Acta Crystallographica*, 17, 781–782.
- Kostiner, E. and Rea, J.R. (1974) Crystal structure of ferrous phosphate, $\text{Fe}_3(\text{PO}_4)_2$. *Inorganic Chemistry*, 13, 2876–2880.
- Lacroix, A. (1902) Note préliminaire sur une nouvelle espèce minérale. *Bulletin de la Société française de Minéralogie*, 25, 85–86.
- McKie, D. (1965) The magnesium aluminum borosilicates: kornerupine and grandidierite. *Mineralogical Magazine*, 34, 346–357.
- Oberti, R. (2001) The diffraction experiment in the study of solid solutions: Long-range properties. *EMU Notes in Mineralogy*, 3, 179–205.
- Olesch, M. and Seifert, F. (1976) Synthesis, powder data and lattice constants of grandidierite, $(\text{Mg},\text{Fe})\text{Al}_3\text{SiBO}_9$. *Neues Jahrbuch für Mineralogie Monatshefte*, 11, 513–518.
- Peacor, D.R., Rouse, R.C., and Grew, E.S. (1999) Crystal structure of boralsilite and its relation to a family of boroaluminosilicates, sillimanite, and andalusite. *American Mineralogist*, 84, 1152–1161.
- Pouchou, J.L. and Pichoir, F. (1985) PAP $\phi(\rho Z)$ procedure for improved quantitative microanalysis. *Microbeam Analysis*, 1985, 104–106.
- Qiu, Z.-M., Rang, M., Chang, J.-T., and Tan, M.-J. (1990) Mössbauer spectroscopy of grandidierite. *Chinese Science Bulletin*, 35, 43–47.
- Robinson, K., Gibbs, G.V., and Ribbe, P.H. (1971) Quadratic elongation: a quantitative measure of distortion in coordination polyhedra. *Science*, 172, 567–570.
- Seifert, F. and Olesch, M. (1977) Mössbauer spectroscopy of grandidierite, $(\text{Mg},\text{Fe})\text{Al}_3\text{BSiO}_9$. *American Mineralogist*, 62, 547–553.

- Shannon, R.D. (1976) Revised effective ionic radii and systematic studies of interatomic distances in halides and chalcogenides. *Acta Crystallographica*, A32, 751–767.
- Stephenson, D.A. and Moore, P.B. (1968) The crystal structure of grandidierite, $(\text{Mg,Fe})\text{Al}_3\text{SiBO}_6$. *Acta Crystallographica*, B24, 1518–1522.
- Stüwe, K., Braun, H.-M., and Peer, H. (1989) Geology and structure of the Larsemann Hills Area. *Australian Journal of Earth Science*, 36, 219–241.
- Tan, M.-J. and Lee, H.-C. (1988) Discovery of grandidierite in China. *Geological Science and Technology Information*, 7, 30 (in Chinese).
- von Knorring, O., Sahama, T.G., and Lehtinen, M. (1969) A note on grandidierite from Fort Dauphin, Madagascar. *Bulletin of the Geological Society of Finland*, 41, 71–74.
- Werding, G. and Schreyer, W. (1996) Experimental studies on borosilicates and selected borates. In L.M. Anovitz and E.S. Grew, Eds., *Boron: Mineralogy, Petrology and Geochemistry*, 33, p. 117–163. Reviews in Mineralogy, Mineralogical Society of America, Chantilly, Virginia.
- Wong-Ng, W., Siegrist, T., DeTitta, G.T., Finger, L.W., Evans, H.T., Jr., Gabe, E.J., Enright, G.D., Armstrong, J.T., Levenson, M., Cook, L.P., and Hubbard, C.R. (2001) Standard reference material (SRM 1990) for single crystal diffractometer alignment. *Journal of Research of the National Institute of Standards and Technology*, 106, 1071–1094.

MANUSCRIPT RECEIVED MARCH 30, 2006
MANUSCRIPT ACCEPTED DECEMBER 20, 2006
MANUSCRIPT HANDLED BY PAOLA BONAZZI